Noble-metal intercalation process leading to a protected adatom in a graphene hollow site

M. Narayanan Nair,[1] M. Cranney,[1,*] T. Jiang,[2] S. Hajjar-Garreau,[1] D. Aubel,[1] F. Vonau,[1] A. Florentin,[1] E. Denys,[1] M.-L. Bocquet,[2] and L. Simon[1,*]

[1]*Institut de Sciences des Matériaux de Mulhouse IS2M, UMR 7361, CNRS, UNISTRA, and UHA, 3 bis rue A. Werner, 68093 Mulhouse, France*

[2]*Université de Lyon, Laboratoire de Chimie, Ecole Normale Supérieure de Lyon, CNRS, 46 allée d'Italie, 69007 Lyon, France*

(Received 23 May 2016; revised manuscript received 9 July 2016; published 22 August 2016)

In previous studies, we have shown that gold deposited on a monolayer (ML) of graphene on SiC(0001) is intercalated below the ML after an annealing procedure and affects the band structure of graphene. Here we prove experimentally and theoretically that some of the gold forms a dispersed phase composed of single adatoms, being intercalated between the ML and the buffer layer and in a hollow position with respect to C atoms of the ML on top. They are freestanding and negatively charged, due to the partial screening of the electron transfer between SiC and the ML, without changing the intrinsic n-type doping of the ML. As these single atoms decouple the ML from the buffer layer, the quasiparticles of graphene are less perturbed, thus increasing their Fermi velocity. Moreover, the hollow position of the intercalated single Au atoms might lead to spin-orbit coupling in the graphene layer covering IC domains. This effect of spin-orbit coupling has been recently observed experimentally in Au-intercalated graphene on SiC(0001) [D. Marchenko, A. Varykhalov, J. Sánchez-Barriga, Th. Seyller, and O. Rader, Appl. Phys. Lett. **108**, 172405 (2016)] and has been theoretically predicted for heavy atoms, like thallium, in a hollow position on graphene [C. Weeks, J. Hu, J. Alicea, M. Franz, and R. Wu, Phys. Rev. X **1**, 021001 (2011); A. Cresti, D. V. Tuan, D. Soriano, A. W. Cummings, and S. Roche, Phys. Rev. Lett. **113**, 246603 (2014)].

DOI: 10.1103/PhysRevB.94.075427

I. INTRODUCTION

A prerequisite for the development of graphene-based nanoelectronics is the precise control of its functionalization. In the case of epitaxial graphene grown on SiC(0001) (here EG), the graphitic layer on top exhibits a gapless graphenelike electronic structure with n-type doping. This graphene layer is decoupled from its SiC substrate by a graphitic layer at the interface, called the buffer layer (BuL), which is composed of one-third C atoms covalently bonded to the Si atoms of the substrate [1–4]. Despite the presence of the BuL, the SiC substrate still alters the electronic properties of EG by decreasing the mobility of its quasiparticles (QPs) and is responsible for its intrinsic n-type doping [5–7]. One way to functionalize EG is to deposit atoms on top of it, which may intercalate between the different C sheets in this layered structure. This was studied experimentally for different elements, from alkali metals to halogens and lanthanides [1,8–29]. In the case of noble metals, we have investigated the functionalization of EG by deposition of gold in thorough studies using scanning tunneling microscopy (STM) techniques (STM-STS) and by photoelectron spectroscopy (ARPES) [12,30–32]. Upon a specific preparation procedure, gold atoms intercalate below the ML, forming two phases. One phase, labeled AuF, corresponds to the intercalation of a continuous ML of gold. This continuous layer of Au induces p-type doping of the graphene layer on top [12]. The other phase, labeled IC, is due to the formation of small intercalated gold dots almost regularly distributed. We have shown that these intercalated gold dots do not dope the graphene layer on top but still modify its band structure, with a 20% increase in the Fermi velocity (v_f) of the QP, with a mass renormalization around the Dirac point, and with a strong extension of its van Hove singularities. In this study, focusing on the IC domain, we show, with the help of density functional theory (DFT) simulations and complementary experiments (x-ray photoelectron spectroscopy; XPS), that Au dots are due to the aggregation of single Au atoms, freestandingly intercalated between the ML and the BuL. As they partially screen the electron transfer from SiC to the ML on top, they are negatively charged. The huge increase in the Fermi velocity of the QP is discussed and attributed to an increase in the nearest-neighbor hopping potential γ_0. Indeed, the presence of single Au atoms intercalated between the ML and the BuL decouple the ML from its SiC substrate, which is experimentally proved by measuring a strong reduction in the roughness of the graphene layer on IC domains. Moreover, computational methods show that the intercalated single Au atoms are in hollow positions with respect to the graphene atoms on top. This might induce spin-orbit coupling in the graphene layer. Indeed, spin-orbit coupling has been recently studied experimentally in Au-intercalated graphene on SiC(0001) [13] and has been theoretically predicted for heavy atoms, such as thallium, in hollow positions on graphene [33,34]. This might lead to the observation of the quantum spin Hall effect in our system, covered mainly by IC domains.

II. EXPERIMENTAL METHODS

Graphene samples were prepared *in situ* in ultrahigh vacuum (UHV) on n-doped 6H-SiC(0001) as described previously [12,30,32]. The majority of the surface was ML graphene. The deposition of gold on top of these samples was done in UHV as described elsewhere [12,30,32]. Samples were further prepared by several cycles of annealing at 1000 K for 2 min. In-house physical characterizations were performed

*Corresponding authors: marion.cranney@uha.fr; laurent.simon@uha.fr

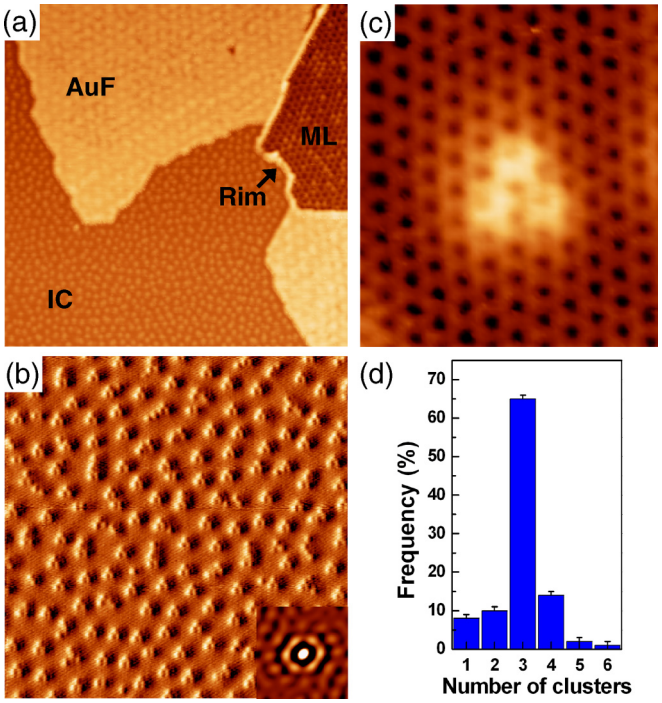

FIG. 1. (a) STM picture showing the two phases (i.e., IC and AuF) due to the intercalation of gold below the graphene monolayer (ML) after several cycles of annealing. (b) Zoom-in of an IC domain, showing that the majority of gold dots are due to the aggregation of three clusters, as shown in the STM image (c). Inset in (b) Its corresponding self-correlation image, showing a quasiperiodic hexagonal arrangement of Au dots. (d) Graph of the distribution of the number of clusters per Au dots, from five STM images totaling more than 500 dots. (a) 86×86 nm^2, -1.5 V; (b) 26×26 nm^2, -2.2 V, $\partial z/\partial x$-derivative representation of the topography; (c) 2.3×2.7 nm^2, -1.5 V (image processing using Gwyddion and WSxM software [46]).

in UHV by scanning tunneling microscopy and by photoelectron spectroscopy techniques (XPS). STM experiments were performed *in situ* with an LT-STM from Omicron at 77 K at a base pressure in the 10^{-11} mb range. Images were acquired in constant-current mode with bias voltage applied to the sample and employing chemically etched W tips. XPS measurements were performed *in situ* using a VG Scienta R3000 spectrometer equipped with a monochromatized Al Kα x-ray source (1486.6 eV) and a hemispherical analyzer. At this high photon energy, our measurements probe not only the surface but also the SiC substrate, and thus the C 1s and the Si 2p spectra have higher SiC bulk signals than in the literature [4,7,35–38]. The electron energy analyzer operated at a 100-eV pass energy. Spectra were measured at both grazing and normal (not shown here) incidence. Shirley background was subtracted from the C 1s, Si 2p, and Au 4f spectra. We used a Lorentzian asymmetric lineshape (LF) for metallic and graphitic core level peaks and a symmetric Voigt lineshape (GL) for the other peaks in the fitting procedure using CasaXPS software [4,35]. For XPS measurements, we used homogeneous samples with a surface covered by 5% $\pm$ 3% ML, 10% $\pm$ 5% AuF, and 82% $\pm$ 5% IC domains, as shown in Figs. 1(a) and 1(b) of Nair *et al.* [32]. Some three-dimensional islands of Au are still present on the surface of the sample after the annealing procedure, but they are scarce. The gold intercalated samples are extremely stable (no change in the gold structures) at room temperature for several months and they remain quite clean even after several weeks in an ambient atmosphere. The contamination after several months in an ambient atmosphere is completely removed by annealing in UHV at 900 K for several hours. This means that the graphene layer protects the intercalated gold structures from contamination, degradation,s and desorption, even when heated at 900 K.

III. METHODOLOGY OF CALCULATIONS

Calculations were carried out within the framework of DFT implemented in the Vienna Ab initio Simulation Package (VASP) [39,40]. The local density approximation was considered to describe the exchange and correlation energy. In order to get a good understanding of the EG substrate, our model was based on a (13×13) graphene on a $(6\sqrt{3}\times6\sqrt{3})$ SiC substrate, instead of a smaller model without the proper large commensurability like (2×2) graphene on a $(\sqrt{3}\times\sqrt{3})$ SiC substrate, which gives 8% extra strain due to the mismatch of graphene and SiC lattice constants. The SiC substrate was modeled by two SiC bilayers, the top face being Si and the bottom being C saturated with hydrogen atoms, including 432 atoms. All structures were relaxed until the total forces were lower than 0.02 eV/Å. STM images at constant current were simulated by means of the Tersoff-Hamann theory [41,42]. An implementation [43,44] was used in order to correctly reproduce the exponential decay of wave functions in the vacuum region: above a given height (approximately 23 Å from the outermost atoms of the sample), the analytical expression of the wave function for a flat potential in vacuum was considered.

IV. RESULTS

The STM image in Fig. 1(a) is a scan area representative of the EG surface after the intercalation of gold atoms. AuF corresponds to the intercalation of a monolayer of Au and IC is due to the formation of small intercalated Au dots. These dots are two-dimensional (2D) and lie flat, parallel to the surface below the ML [12]. As shown in the STM images in Figs. 1(a) and 1(b), the dots are homogeneously distributed all over the IC domains, even when adjoining a rim or a AuF domain. They form a quasiperiodic hexagonal arrangement of aggregates of clusters, with a measured mean distance of 2.25 $\pm$ 0.07 nm between the centers of mass of two neighboring dots and of 4.17 $\pm$ 0.05 Å between two clusters inside a dot (see Fig. 5 as well). These distances are always identical and not related to the deposited quantity of Au or the size of the IC domain (see Supplemental Material Fig. 1 [45]). Most of the dots are formed by three clusters, as shown in Figs. 1(b) to 1(d). An individual cluster is shown in Fig. 2(a). As can be seen, an individual cluster has an almost-triangular shape and it affects the contrast of 9 C atoms on top. In order to understand in more detail the composition of these clusters and their positions below the ML, a theoretical study was performed to compare the experimental STM images and the simulated STM images, as shown in Fig. 2. Several

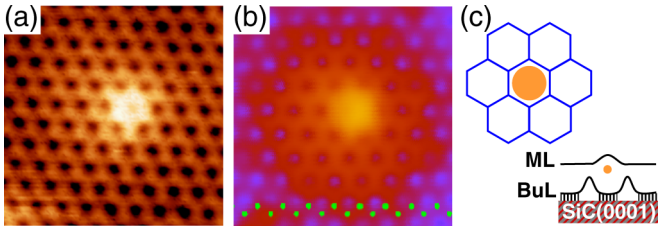

FIG. 2. Direct comparison of (a) the experimental STM image with (b) the simulated STM image of an individual Au atom intercalated between the ML and the BuL. Image (a), 2.1×2.1 nm^2, wa made at -1.1 V. Image (b), simulated at -1.3 V, is the same size as (a), with the C atoms of the ML on top of the Au atom displayed in green. (c) The hollow position of the intercalated Au atom.

situations were tested, changing the size of the 2D Au clusters (from Au_6 clusters to single Au atoms) and changing their positions, i.e., intercalated between the ML and the BuL or intercalated below the BuL (see simulated STM images of all these possible cases in Supplemental Material Fig. 2 [45]). Among all the simulated situations, only that of a single Au atom intercalated between the ML and the BuL shows a simulated STM image very similar to the experimental one, with the same shape and the same number of affected C atoms on top, as shown in Fig. 2(b). Thus we may infer that IC domains are made of single Au atoms intercalated between the BuL and the ML. Moreover, the calculations show that the Au atom is nearly in a hollow position with respect to C atoms on top, i.e., nearly in the center of the hexagon as depicted in Figs. 2(c) and 3(a). The measured mean distance of 4.17 ± 0.05 Å between two Au atoms inside a dot means that all Au atoms remain single and are in hollow positions inside a dot. The hollow position of the single Au atoms is highly important for the graphene functionalization and, notably, for the observation of the quantum spin Hall effect in such system. Indeed, such an adatom position might lead to the induction of spin-orbit coupling in the graphene layer, as theoretically predicted for heavy atoms, like thallium [33,34].

The freestanding nature of the intercalated single Au atom is shown by the calculated differential charge density plot [see Fig. 3(b)]: there is no significant charging of either BuL or ML and no shared electrons between Au atom and C or Si atom counterparts. This points to the absence of a chemical bond between Au and ML, BuL, or SiC. The charge redistribution after Au intercalation between the ML and the BuL shows a dual behavior of the single Au atom: the diffuse s shell gains electrons, while the contracted out-of-plane d shells lose electrons. The net charge on the intercalated Au atom can be roughly evaluated by comparing the atomic charge of Au before and after intercalation: it amounts to $0.25e$. Hence the DFT analysis shows that a single Au atom intercalated between the BuL and the ML is freestanding and slightly negatively charged. In order to support this assertion, we perform *in situ* XPS measurements on samples prior to and after Au deposition (covered then by 82% IC domains). There should be no formation of Au-C covalent bonds, as Au and C atoms have almost the same electronegativity, and hence only Au-Si bonds can be formed. Gierz *et al.* came to the conclusion that Au atoms intercalated below the BuL are

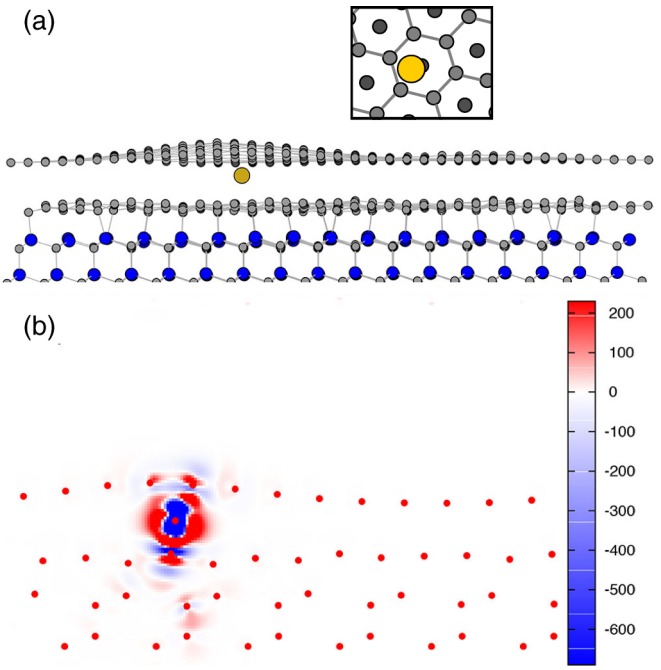

FIG. 3. (a) Side view of the DFT optimized structure of a single Au atom intercalated between the BuL and the ML. The Au atom is displayed in yellow, the C in gray, and the Si in blue. Inset: Corresponding top view, showing the position of the intercalated single Au atom: nearly at a hollow site with respect to the ML (distance of 2.40 Å; C atoms displayed in light gray) and nearly at a top site with respect to the BuL (distance of 2.06 Å; C atoms in dark gray). The BuL-to-ML distance varies from 3.20 to 4.20 Å. (b) Charge density difference upon intercalation of a single Au atom between the BuL and the ML. Red (blue) regions mark accumulation (depletion) of electrons. Units are $10^{-3}e$.

bonded to Si atoms of the SiC substrate, thus altering the BuL or decoupling it from the SiC substrate [47]. However, the deposition of Au was done in their case before the full formation of an ML. We present in Fig. 4 the C $1s$ and the Si $2p$ spectra obtained both for the pristine EG samples prior to Au deposition (measured spectra in red) and for our samples covered by 82% IC domains (measured spectra in black) for comparison. The deconvolutions of the different spectra are shown in Supplemental Material Fig. 3 [45] and the positions of the deconvoluted peaks are listed in Supplemental Material Table 1 [45]. Note that the positions of the peaks of pristine EG are in good agreement with the data reported in Refs. [4,7], and [35–38]. As shown directly in Fig. 4, the C $1s$ and Si $2p$ spectra of pristine EG and of IC domains are nearly identical and not shifted in binding energy (BE) as expected, as Au dots do not dope the graphene layer [12,32]. The insets in the C $1s$ and Si $2p$ spectra in Fig. 4 present the deconvoluted peaks related to the BuL (i.e., the ones labeled S1 and S2 in the C $1s$ spectra related to the sp^3 and sp^2 C atoms of the BuL, respectively, and the one labeled $6\sqrt{3}$ for the Si $2p$ spectra), whose positions and areas are unchanged prior to and after Au intercalation. This means that the BuL is not altered and not decoupled from its SiC substrate by intercalated Au atoms. Moreover, we can safely exclude the formation of gold silicide, as this should

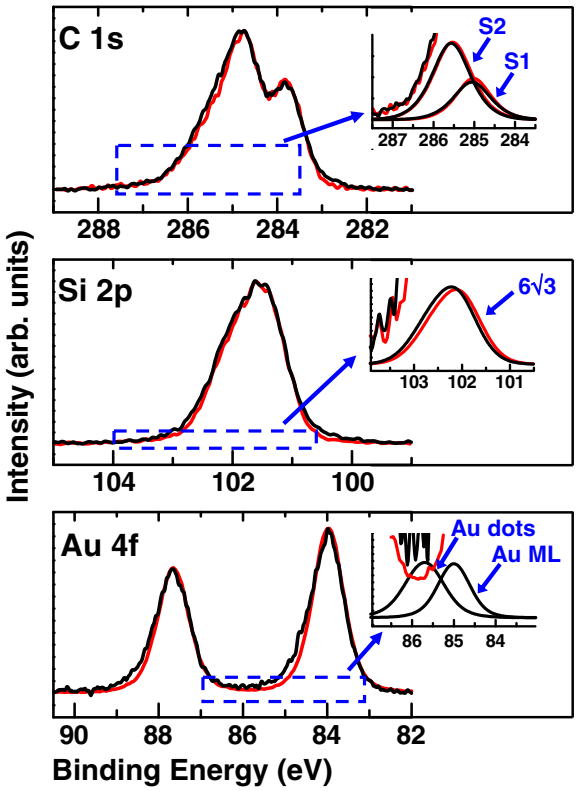

FIG. 4. C 1s and Si 2p spectra measured on pristine EG (experimental data are displayed in red) and in IC domains (in black) are presented for direct comparison. Insets: Deconvoluted peaks related to the BuL for both spectra. We also show two Au 4f spectra, the one in red being measured on a clean Au(111) surface as a reference [50] and the other one, in black, measured on IC domains. Inset: The two deconvoluted peaks from the IC-domain spectrum, one related to the intercalated monolayers of Au from the AuF domains (Au ML) and the other to the intercalated Au 2D dots (Au dots). The deconvolutions of all spectra are shown in Supplemental Material Fig. 3 [45] and the positions of all deconvoluted peaks are listed in Supplemental Material Table 1 [45]. See text for details.

drastically change the peaks related to the BuL in C 1s and Si 2p spectra of IC domains (i.e., a strong decrease in their areas) and as another peak should appear in the Si 2p spectrum at a BE of around 99.9 eV, following Refs. [48] and [49]. We present in Fig. 4 a detailed analysis of the chemical states of deposited gold by comparing two Au 4f spectra, the one in red being measured on a clean Au(111) surface as a reference [50] and the other one, in black, measured in IC domains. The deconvolutions of the different spectra are shown in Supplemental Material Fig. 3 [45] and the positions of the deconvoluted peaks are listed in Supplemental Material Table 1 [45]. The reference Au 4$f_{7/2}$ spectrum and the one measured in IC domains differ only at a BE around 85 eV due to the presence in the IC-domain spectrum of two additional peaks that are probably related to the formation of intercalated Au nanoparticles and not due to the formation of Au silicide, in agreement with Ref. [51]. Indeed, when decreasing the size of a Au nanoparticle, its related Au 4$f_{7/2}$ peak shifts towards a higher BE due to two coexisting effects: the initial-state and the final-state effects [51–56]. Thus, the peak at a lower BE is related to MLs of Au in AuF domains, and the peak at a higher BE to Au dots in IC domains, as shown in the inset in Fig. 4. Therefore, we can conclude that single Au atoms of IC domains are freestanding, being intercalated between the BuL and the ML.

As gold atoms have a high positive electron affinity and a relatively high first ionization potential, they have a tendency to attract electrons, leading to screening of the transfer of charge from the SiC to the graphene layer. Thus p-type doping of graphene is expected, as measured experimentally [11,12]. Previous STS and ARPES measurements have shown that intercalated Au dots did not dope the graphene layer, as there was no change in the position of the Dirac point E_D prior to versus after Au intercalation [12,32,57]. In addition, ARPES measurements revealed an increase in the Fermi velocity (v_f) of the QPs in IC domains from $0.99 \pm 0.08 \times 10^6$ to $1.24 \pm 0.2 \times 10^6$ m $\cdot$ s^{-1} [32]. Even if the screening of the charge transfer from the SiC to the graphene layer by single Au atoms is not effective enough to dope it, Au atoms attract electrons from SiC. This was confirmed by calculations [see the differential charge density plot in Fig. 3(b)]. We estimate the transfer of charge per intercalated Au atom by using the variation of the density of electrons n_e at the Fermi energy in relation to E_D and v_f [58]:

$$n_e = \frac{E_D^2}{\pi \hbar^2 v_f^2}. \quad (1)$$

Following Eq. (1), the estimated electron density at the Fermi energy is 6.22×10^{12} cm^{-2} for a pristine ML and 2.57×10^{12} cm^{-2} for an IC domain, respectively, using the values of E_D and v_f obtained from our ARPES measurements [32]. This means that the transfer of electrons from SiC to intercalated single Au atoms is 3.65×10^{12} cm^{-2}. If we assume homogeneous coverage of the IC domain, with a hexagonal arrangement of Au dots (distance between Au dots of 2.25 nm) consisting of three single Au atoms, then each Au atoms has attracted 5.33×10^{-2} electrons. This estimated electron transfer is higher than those for Bi and Sb atoms [11], which is expected, as Au has a higher electronegativity than Sb and Bi. From our experiments, we can conclude that freestanding single Au atoms of IC domains intercalated between the BuL and the ML are negatively charged. This raises the question of the driving force of their self-organization, for example, possible Coulomb interactions, as they are freestanding.

We obtain further information about the interactions between negatively charged Au dots by studying the topographic STM images, as shown in Fig. 5. At first glance, the distribution of Au dots in IC domains may appear random, but self-correlation images, such the insets in Figs. 1(b) and 5(a), show some order. There is a clear sixfold pattern due to the superimposition of an isotropic ring on a hexagonal pattern of six spots, as in the case of a hexatic phase in melted 2D crystals [59–61]. This phase is between a 2D crystal and an isotropic liquid, showing quasi-long-range order in the orientation of nearest-neighbor pairs of Au dots (as in a 2D solid) and short-range positional order of Au dots (as in a 2D liquid). In our case, the exponential decay [$\propto \exp(-0.997r)$] of the pair distribution function $f(r)$ obtained using Fiji [62,63] prove that the positional order

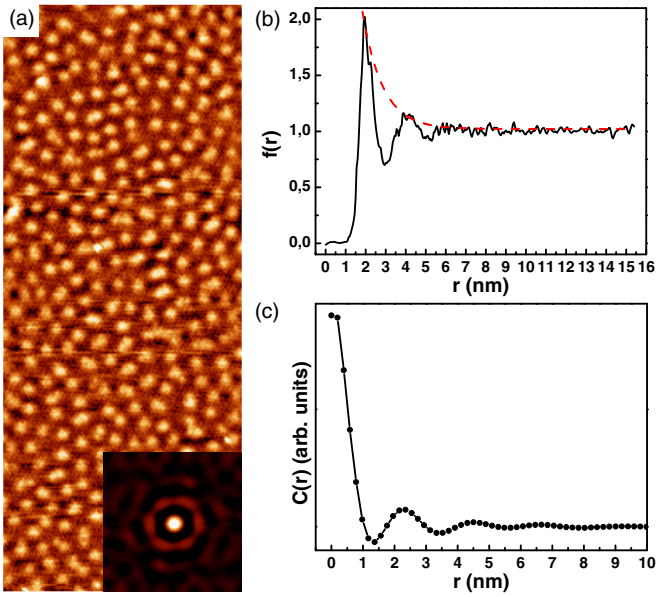

FIG. 5. (a) STM picture of an IC domain, with its corresponding self-correlation image in the inset, showing a quasiperiodic hexagonal arrangement of Au dots. (b) Pair distribution function, $f(r)$, whose envelope decays exponentially [$\propto \exp(-0.997r)$; fit shown by dashed red line]. (c) Graph of the self-correlation function of the atomic positions, $C(r)$, which stems from a radially averaged self-correlation image of an STM picture. From $C(r)$, we measure a mean distance between the centers of mass of two neighboring Au dots of 2.25 ± 0.07 nm. These measurements, using Fiji [62,63] for $f(r)$ and WSxM for $C(r)$, were made on 14 STM images at different bias voltages, using different tips and on different samples. Image (a): 22.7×55.6 nm^2, -1.5 V.

is indeed only short range [see Fig. 5(b)]. The first peak in the averaged self-correlation function of the atomic positions $C(r)$ (obtained using WSxM) corresponds to the mean nearest-neighbor distance between Au dots. This large distance, 2.25 ± 0.07 nm, implies that the interactions between Au dots are long-range, like repulsive dipole-dipole electrostatic interactions [64,65] or indirect electrostatic interactions mediated by electrons from the environment (from graphene, the BuL, or SiC) [61,66–69]. We perform classical molecular dynamics simulations using LAMMPS software [70] to check whether the spatial distribution of Au dots is due only to direct interactions between them. The simulations are performed assuming Lennard-Jones and electrostatic (Coulomb, charge-dipole, dipole-dipole) interactions between the Au dots only, which are treated as a microcanonical ensemble and approximated as spherical pseudoatoms carrying a charge and/or a point dipole moment [71]. The simulations generate the pair distribution function $f(r)$, directly compared to the experimental one displayed in Fig. 5(b). Two criteria must be fulfilled in order to judge the level of reliability of the simulation: the positions of the peaks of $f(r)$ (which correspond to the representative distances between Au dots) and the amplitudes of the peaks (which represent the probability of measuring those specific distances) must be the same as the experimental values. Whatever the temperature of the thermostat, we never obtain a pair distribution function exactly the same as the experimental one using realistic values (based on our ARPES experiments) of charge (from 5.33×10^{-2} to 0.1 electron per Au atom) and of dipole moment (from 0 to 8 D). Thus we cannot exclude any influence of the simulated direct repulsive long-range interactions on the observed distances between Au dots, but the environment (graphene, the BuL, and/or SiC) should also have an effect on the repartition of Au dots. There must indeed be an influence of the BuL on the repartition of Au dots, as the measured distance of 2.25 ± 0.07 nm is quite close to the length of the hexagons (2.13 nm) due to the $(6\sqrt{3} \times 6\sqrt{3})$ R30-SiC reconstruction of the BuL [5,72] and not directly related to the periodicity of the SiC substrate or of the graphene layer.

In our previous studies, we have found that intercalated single Au atoms have a great impact on the band structure of EG, with a strong extension of the van Hove singularities and a 20% increase in v_f [30–32]. There are two possible reasons for this increase in v_f, either an increase in the lattice parameter a_G of the ML on top or an increase in the nearest-neighbor hopping energy γ_0, i.e., the amplitude of the probability of a QP's tunneling between two neighboring lattice sites [73]. Indeed, v_f is proportional to both parameters in the first approximation

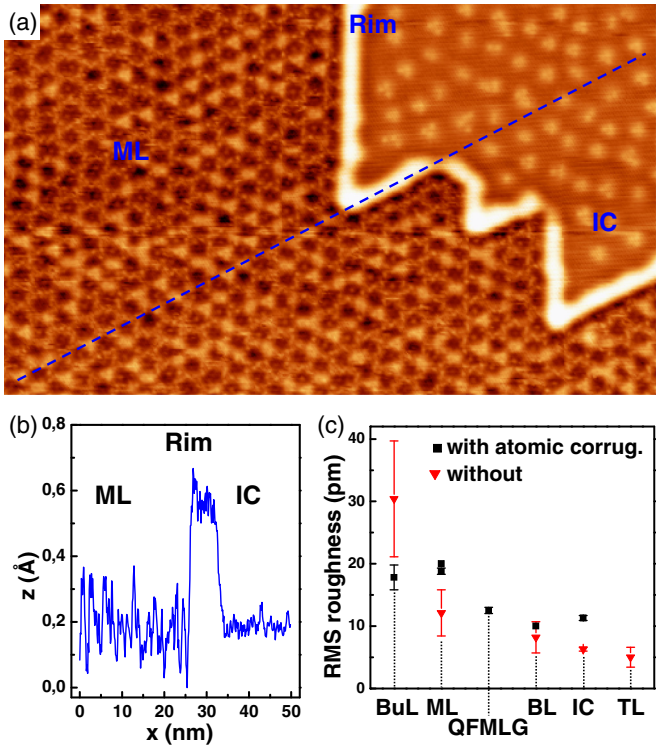

FIG. 6. (a) STM picture showing an IC domain separated from a pristine ML by a rim. (b) Profile curve corresponding to the dashed blue line in the STM image. One can directly see that the graphene layer in the IC domain is almost flat between intercalated Au dots. (c) Root-mean-square roughness of different graphene layers: BuL, pristine ML; QFMLG, ML with intercalated H atoms [75]; BL, pristine bilayer graphene; and TL, pristine trilayer graphene. Some were measured without removing the atomic corrugation (black squares), whereas red triangles represent measurements of the "real" roughness of the layer. This figure is adapted from Refs. [6,74], and [75]. Image (a): 45.4×27.2 nm^2, -1.3 V.

as given by Eq. (2):

$$v_f = \frac{\sqrt{3}}{2\hbar}\,\gamma_0 a_G. \tag{2}$$

We measured a_G in a pristine ML and in IC domains in the same STM images at different bias voltages and found no variation of a_G greater than 4%. Consequently, we attribute this increase in v_f to an increase in γ_0. This means that the intercalation of single Au atoms between the ML and the BuL induces fewer perturbations of the QPs of the ML on top, which is counterintuitive, as we have already shown that QPs are scattered in IC domains at a specific energy range [30]. The fact that the QPs of the ML are less perturbed is actually due to the better decoupling of the graphene layer on top of the IC domains from the BuL, as shown in Fig. 6. Indeed, Figs. 6(a) and 6(b) display the BuL-induced corrugation of a pristine ML [5,6] and that of an IC domain, showing that the roughness of IC domains is much reduced, the graphene layer in IC domains being almost flat between Au dots (the roughness here is due only to the atomic corrugation). Figure 6(c) shows that the measured roughness of IC domains is even below that of ML graphene decoupled from a SiC substrate by hydrogen intercalation below BuL (labeled QFMLG) [75] and equal to that of pristine trilayer graphene on SiC(0001) within measurement uncertainty [6,74] (see Supplemental Material Fig. 4 [45] for a detailed analysis of the root-mean-square roughnesses of a pristine ML, an IC domain, and an ML between Au dots in an IC domain depending on the applied bias voltage). Negatively charged single atoms of Au, freestandingly intercalated between the BuL and the ML, thus improve the electronic properties of graphene by decoupling it from its SiC substrate. We report here a new way to obtain a quasi-ideal freestanding graphene on a SiC(0001) substrate.

V. CONCLUSIONS

The deposition and subsequent annealing of Au on EG lead to the intercalation of Au atoms below the ML. Some of them form a specific type of domain, called the IC domain, made of almost regularly distributed Au dots that do not dope the graphene layer on top. From experiments and computational methods, we have shown that these Au dots are made of single Au atoms (usually three), freestandingly intercalated between the BuL and the ML, and are negatively charged, as they partially screen the electron transfer from SiC to the graphene layer on top. Their distribution between the BuL and the ML is not random but probably due to interactions mediated by electrons from the environment, particularly with the BuL. Former ARPES measurements have shown an increase in v_f due to the presence of intercalated Au dots. This effect has finally been attributed to an increase in the nearest-neighbor hopping potential γ_0 due to the decoupling of the ML from the BuL, which has been experimentally proved. We report here a new way to decouple graphene from its SiC(0001) substrate, which leads to an improvement in its electronic properties. Moreover, computational methods show that the intercalated single Au atoms are in hollow positions with respect to the graphene atoms on top, which might induce spin-orbit coupling in the graphene layer. This effect of spin-orbit coupling has been proved experimentally on Au-intercalated graphene on SiC(0001) [13] and has been theoretically predicted for heavy atoms, such as thallium, in hollow positions on graphene [33,34]. This might lead to the observation of the quantum spin Hall effect in our system, covered mainly by IC domains.

ACKNOWLEDGMENTS

We thank L. Daukiya for the preparation of epitaxial graphene samples for x-ray photoelectron spectroscopy measurements. M.C. thanks J. Renard (Néel Institut) and, particularly, I. Deroche (IS2M) for very useful discussions about molecular dynamics simulations using LAMMPS. She thanks also A. Kohlmeyer and S. Plimpton, LAMMPS developers at Sandia National Laboratories and Temple University, respectively, for their corrections of the simulation's program. This work was supported by the Région Alsace and the CNRS. The Agence Nationale de la Recherche supported this work under the ANR Blanc program, reference ANR-2010-BLAN-1017-ChimiGraphN.

[1] T. Ohta, A. Bostwick, Th. Seyller, K. Horn, and E. Rotenberg, Science **313**, 951 (2006).
[2] S. Y. Zhou, G.-H. Gweon, A. V. Federov, P. N. First, W. A. de Heer, D.-H. Lee, F. Guinea, A. H. Castro Neto, and A. Lanzara, Nat. Mater. **6**, 770 (2007).
[3] L. Vitali, C. Riedl, R. Ohmann, I. Brihuega, U. Starke, and K. Kern, Surf. Sci. **602**, L127 (2008).
[4] C. Riedl, C. Coletti, and U. Starke, J. Phys. D: Appl. Phys. **43**, 374009 (2010).
[5] F. Varchon, P. Mallet, J.-Y. Veuillen, and L. Magaud, Phys. Rev. B **77**, 235412 (2008).
[6] P. Lauffer, K. V. Emtsev, R. Graupner, Th. Seyller, L. Ley, S. A. Reshanov, and H. B. Weber, Phys. Rev. B **77**, 155426 (2008).
[7] K. V. Emtsev, F. Speck, Th. Seyller, L. Ley, and J. D. Riley, Phys. Rev. B **77**, 155303 (2008).
[8] M. Batzill, Surf. Sci. Rep. **67**, 83 (2012).
[9] Q. Tang, Z. Zhou, and Z. Chen, Nanoscale **5**, 4541 (2013).
[10] X. Liu, Y. Han, J. W. Evans, A. K. Engstfeld, R. J. Behm, M. C. Tringides, M. Hupalo, H.-Q. Lin, L. Huang, K.-M. Ho, D. Appy, P. A. Thiel, and C.-Z. Wang, Prog. Surf. Sci. **90**, 397 (2015).
[11] I. Gierz, C. Riedl, U. Starke, C. R. Ast, and K. Kern, Nano Lett. **8**, 4603 (2008).
[12] B. Premlal, M. Cranney, F. Vonau, D. Aubel, D. Casterman, M. M. De Souza, and L. Simon, Appl. Phys. Lett. **94**, 263115 (2009).
[13] D. Marchenko, A. Varykhalov, J. Sánchez-Barriga, Th. Seyller, and O. Rader, Appl. Phys. Lett. **108**, 172405 (2016).
[14] C. Virojanadara, S. Watcharinyanon, A. A. Zakharov, and L. I. Johansson, Phys. Rev. B **82**, 205402 (2010).
[15] S. Watcharinyanon, C. Virojanadara, and L. I. Johansson, Surf. Sci. **605**, 1918 (2011).

[16] A. L. Walter, K.-J. Jeon, A. Bostwick, F. Speck, M. Ostler, T. Seyller, L. Moreschini, Y. S. Kim, Y. J. Chang, K. Horn, and E. Rotenberg, Appl. Phys. Lett. **98**, 184102 (2011).

[17] K. V. Emtsev, A. A. Zakharov, C. Coletti, S. Forti, and U. Starke, Phys. Rev. B **84**, 125423 (2011).

[18] T. Gao, Y. Gao, C. Chang, Y. Chen, M. Liu, S. Xie, K. He, X. Ma, Y. Zhang, and Z. Liu, ACS Nano **6**, 6562 (2012).

[19] A. Sandin, T. Jayasekera, J. E. Rowe, K. W. Kim, M. B. Nardelli, and D. B. Dougherty, Phys. Rev. B **85**, 125410 (2012).

[20] C. Xia, S. Watcharinyanon, A. A. Zakharov, R. Yakimova, L. Hultman, L. I. Johansson, and C. Virojanadara, Phys. Rev. B **85**, 045418 (2012).

[21] S. Watcharinyanon, L. I. Johansson, C. Xia, J. I. Flege, A. Meyer, J. Falta, and C. Virojanadara, Graphene **2**, 66 (2013).

[22] Z.-J. Wang, M. Wei, L. Jin, Y. Ning, L. Yu, Q. Fu, and X. Bao, Nano Res. **6**, 399 (2013).

[23] J. Baringhaus, A. Stöhr, S. Forti, S. A. Krasnikov, A. A. Zakharov, U. Starke, and C. Tegenkamp, Appl. Phys. Lett. **104**, 261602 (2014).

[24] L. H. de Lima, R. Landers, and A. de Siervo, Chem. Mater. **26**, 4172 (2014).

[25] K. Yagyu, T. Tajiri, A. Kohno, K. Takahashi, H. Tochihara, H. Tomokage, and T. Suzuki, Appl. Phys. Lett. **104**, 053115 (2014).

[26] S. J. Sung, J. W. Yang, P. R. Lee, J. G. Kim, M. T. Ryu, H. M. Park, G. Lee, C. C Hwang, K. S. Kim, J. S. Kim, and J. W. Chung, Nanoscale **6**, 3824 (2014).

[27] C. Xia, L. I. Johansson, Y. Niu, A. A. Zakharov, E. Janzén, and C. Virojanadara, Carbon **79**, 631 (2014).

[28] C. Xia, L. I. Johansson, A. A. Zakharov, L. Hultman, and C. Virojanadara, Mater. Res. Exp. **1**, 015606 (2014).

[29] H. Kim, O. Dugerjav, A. Arvisbaatar, and J. M. Seo, New J. Phys. **17**, 083058 (2015).

[30] M. Cranney, F. Vonau, P. B. Pillai, E. Denys, D. Aubel, M. M. De Souza, C. Bena, and L. Simon, Europhys. Lett. **91**, 66004 (2010).

[31] L. Simon, C. Bena, F. Vonau, M. Cranney, and D. Aubel, J. Phys. D: Appl. Phys. **44**, 464010 (2011).

[32] M. N. Nair, M. Cranney, F. Vonau, D. Aubel, P. Le Fèvre, A. Tejeda, F. Bertran, A. Taleb-Ibrahimi, and L. Simon, Phys. Rev. B **85**, 245421 (2012).

[33] C. Weeks, J. Hu, J. Alicea, M. Franz, and R. Wu, Phys. Rev. X **1**, 021001 (2011).

[34] A. Cresti, D. V. Tuan, D. Soriano, A. W. Cummings, and S. Roche, Phys. Rev. Lett. **113**, 246603 (2014).

[35] C. Riedl, Dissertation, University Erlangen-Nürnberg (2010); opus4.kobv.de/opus4-fau/frontdoor/index/index/docId/1364, and references therein.

[36] L. I. Johansson, F. Owman, and P. Mårtensson, Surf. Sci. **360**, L483 (1996).

[37] K. V. Emtsev, A. Bostwick, K. Horn, J. Jobst, G. L. Kellogg, L. Ley, J. L. McChesney, T. Ohta, S. A. Reshanov, J. Röhrl, E. Rotenberg, A. K. Schmid, D. Waldmann, H. B. Weber, and T. Seyller, Nat. Mater. **8**, 203 (2009).

[38] K. V. Emtsev, Dissertation, University Erlangen-Nürnberg (2009); opus4.kobv.de/opus4-fau/frontdoor/index/index/docId/883.

[39] G. Kresse, Phys. Rev. B **47**, 558 (1993).

[40] G. Kresse and J. Hafner, Phys. Rev. B **49**, 14251 (1994).

[41] J. Tersoff and D. R. Hamann, Phys. Rev. Lett. **50**, 1998 (1983).

[42] J. Tersoff and D. R. Hamann, Phys. Rev. B **31**, 805 (1985).

[43] M. Rohlfing, R. Temirov, and F. S. Tautz, Phys. Rev. B **76**, 115421 (2007).

[44] N. Lorente, Dynamics **3**, 575 (2008).

[45] See Supplemental Material at http://link.aps.org/supplemental/10.1103/PhysRevB.94.075427 for complementary STM measurements (for example, the complete roughness analysis). It also reports the deconvolutions of the different C $1s$, Si $2p$, and Au $4f$ spectra from XPS measurements. Finally, it includes all the simulated STM images of the different cases (from Au_6 clusters to single atoms, intercalated either below the buffer layer or between the buffer layer and the monolayer graphene).

[46] I. Horcas, R. Fernández, J. M. Gómez-Rodríguez, J. Colchero, J. Gómez-Herrero, and A. M. Baro, Rev. Sci. Instrum. **78**, 013705 (2007).

[47] I. Gierz, T. Suzuki, R. T. Weitz, D. S. Lee, B. Krauss, C. Riedl, U. Starke, H. Höchst, J. H. Smet, C. R. Ast, and K. Kern, Phys. Rev. B **81**, 235408 (2010).

[48] C. Virojanadara and L. I. Johansson, Surf. Sci. **600**, 436 (2006).

[49] D. Stoltz, S. E. Stoltz, and L. S. O. Johansson, J. Phys.: Condens. Matter **19**, 266006 (2007).

[50] The Au $4f$ reference spectrum was made on a Au(111) surface of a monocrystal, which was cleaned and annealed *in situ* in UHV. In-house x-ray photoelectron spectroscopy was performed in UHV using the same conditions as for the measurement of the Au $4f$ spectrum in IC domains, as reported under Experimental Methods (our VG Scienta R3000 spectrometer equipped with a monochromatized Al Kα x-ray source and a hemispherical analyzer 100-eV pass energy grazing incidence). We used a Lorentzian asymmetric lineshape (LF) and a Shirley background in the fitting procedure using CasaXPS software.

[51] Z.-J. Wang, Q. Fu, Z. Wang, and X. Bao, Surf. Sci. **606**, 1313 (2012).

[52] M. G. Mason, Phys. Rev. B **27**, 748 (1983).

[53] H.-G. Boyen, A. Ethirajan, G. Kästle, F. Weigl, and P. Ziemann, Phys. Rev. Lett. **94**, 016804 (2005).

[54] M. Büttner and P. Oelhafen, Surf. Sci. **600**, 1170 (2006).

[55] M. Turner, V. B. Golovko, O. P. H. Vaughan, P. Abdulikn, A. Berenguer-Murcia, M. S. Tikhov, B. F. G. Johnson, and R. M. Lambert, Nature **454**, 981 (2008).

[56] Y. Kitsudo, A. Iwamoto, H. Matsumoto, K. Mitsuhara, T. Nishimura, M. Takizama, T. Akita, Y. Maeda, and Y. Kido, Surf. Sci. **603**, 2108 (2009).

[57] The position of the Dirac point E_D measured by STS dI/dV curves on a pristine ML and in the IC domain is the same, at around -0.5 eV [12]. By ARPES, we measured the E_D at -288 meV for the pristine ML and at -232 meV for the IC domain [32]. The discrepancy in the energy level of E_D between STS and ARPES measurements is probably due to the partial oxidation of the graphene sample during ARPES measurements, as they were done *ex situ*, whereas STS measurements were done *in situ* [4,35].

[58] N. W. Ashcroft and N. D. Mermin, *Solid State Physics* (Thomson Learning, 1976).

[59] K. J. Strandburg, Rev. Mod. Phys. **60**, 161 (1988).

[60] B.-J. Lin and L.-J. Chen, Colloids Surf. A **284-285**, 239 (2006).

[61] M. Ternes, M. Pivetta, F. Patthey, and W.-D. Schneider, Prog. Surf. Sci. **85**, 1 (2010).

[62] J. Schindelin, I. Arganda-Carreras, E. Frise, V. Kaynig, M. Longair, T. Pietzsch, S. Preibisch, C. Rueden, S. Saalfeld, B. Schmid, J.-Y. Tinevez, D. J. White, V. Hartenstein,

K. Eliceiri, P. Tomancak, and A. Cardona, Nat. Meth. **9**, 676 (2012).

[63] C. A. Schneider, W. S. Rasband, and K. W. Eliceiri, Nat. Meth. **9**, 671 (2012).

[64] J. Renard, M. B. Lundeberg, J. A. Folk, and Y. Pennec, Phys. Rev. Lett. **106**, 156101 (2011).

[65] C.-L. Song, B. Sun, Y.-P. Jiang, L. Wang, K. He, X. Chen, P. Zhang, X.-C. Ma, and Q.-K. Xue, Phys. Rev. Lett. **108**, 156803 (2012).

[66] X. Liu, C. Z. Wang, M. Hupalo, W.-C. Lu, P. A. Thiel, K. M. Ho, and M. C. Tringides, Phys. Rev. B **84**, 235446 (2011).

[67] S. M. Binz, M. Hupalo, X. Liu, C. Z. Wang, W.-C. Lu, P. A. Thiel, K. M. Ho, E. H. Conrad, and M. C. Tringides, Phys. Rev. Lett. **109**, 026103 (2012).

[68] X. Liu, C.-Z. Wang, H.-Q. Lin, K. Chang, J. Chen, and K.-M. Ho, Phys. Rev. B **91**, 035415 (2015).

[69] H.-H. Chen, S. H. Su, S.-L. Chang, B.-Y. Cheng, C.-W. Chong, J. C. A. Huang, and M.-F. Lin, Carbon **93**, 180 (2015).

[70] S. Plimpton, J. Comput. Phys. **117**, 1 (1995); http://lammps.sandia.gov.

[71] The simulations were done in two dimensions, with the pseudoatoms constrained to move on a plane and with the z components of velocities and forces zeroed out every time step. The system was described by a microcanonical ensemble using a Nosé-Hoover thermostat at three temperatures, i.e., 1000 K (temperature of annealing), 300 K, and 77 K (temperature of STM imaging). The 460 Au dots were approximated as finite-size spheres (with a mass corresponding to 3 Au atoms), carrying a charge and/or a point dipole moment perpendicular to the plane. We tried two starting scenarios for the simulations, one with pseudoatoms forming a hexagonal arrangement (with a distance of 2.25 nm between them) and one where the pseudoatoms were disorganized as in a 2D liquid. The simulations generated the pair distribution function $f(r)$, which was directly compared to the experimental one displayed in Fig. 5(b).

[72] S. Kim, J. Ihm, H. J. Choi, and Y.-W. Son, Phys. Rev. Lett. **100**, 176802 (2008).

[73] P. R. Wallace, Phys. Rev. **71**, 622 (1947).

[74] V. W. Brar, Y. Zhang, Y. Yayon, T. Ohta, J. L. McChesney, A. Bostwick, E. Rotenberg, K. Horn, and M. F. Crommie, Appl. Phys. Lett. **91**, 122102 (2007).

[75] S. Goler, C. Coletti, V. Piazza, P. Pingue, F. Colangelo, V. Pellegrini, K. V. Emtsev, S. Forti, U. Starke, F. Beltram, and S. Heun, Carbon **51**, 249 (2013).